ELSEVIER

Journal of Chromatography A, 722 (1996) 157–167

JOURNAL OF CHROMATOGRAPHY A

Measurement precision and $1/f$ noise in analytical instruments

Yuzuru Hayashi*, Rieko Matsuda, Russell B. Poe

National Institute of Health Sciences, 1-18-1 Kami-Yoga, Setagaya, Tokyo 158, Japan

Abstract

The recently promulgated uncertainty theory of instrumental analyses was used to minimize the relative standard deviation of measurements. Naphthalene, acenaphthene, pyrene and perylene in HPLC were used as illustrations. For a Gaussian model peak with a width (S.D., σ) of fifteen data points, the optimum integration domain was about ± 6 data points ($\pm 0.4\sigma$) around the peak centre on the HPLC baseline examined. Two commonly used integration modes were examined: horizontal zero line and oblique zero line. The precision was almost the same for both modes in the HPLC analysis. The signal shape at the limit of detection was also shown for the optimum integration domain. The error accompanying the use of the uncertainty theory was evaluated using a Monte Carlo simulation. The practical applicability and limitations of the theory are discussed.

1. Introduction

Validation of analytical systems, quality assurance, GMP (good manufacturing practice) and GLP (good laboratory practice) often require the specification of the actual instrumental precision, that is, the relative standard deviation (R.S.D.) of measurements of target materials. This statistical quantity, however, cannot be obtained without repeated experiments on the same samples under the same operating conditions. Therefore, prediction of the actual precision, not a model precision, is needed and will have a wide application in analytical chemistry. This theory is not limited to the above examples, including validation and GMP, but is also applicable to the optimization of operating conditions in an analysis. The optimum is defined as the condition that provides the maximum precision among all the examined conditions.

In liquid chromatography, the instrumental uncertainty has been studied for more than two decades [1–16]. Uncertainty equations take the following general expression [2,4,8,11,14,15]:

$$(\text{R.S.D.})^2 = \frac{s_B^2}{A^2} + I^2 \qquad (1)$$

where s_B denotes the standard deviation (S.D.) of the measurement error originating from the baseline drift, A the signal area of a target material and I the independent error that corresponds to the sample injection error. In trace analysis (low values of A), the precision is subject to baseline noise, s_B, and in macroanalysis (high values of A), the injection error, I, is the major cause of the total measurement imprecision. The most difficult to determine in theory and practice is the baseline error, s_B.

Huber et al. [2] determined the measurement error, s_B, from integration output over a period that approximately corresponds to the integration time of a target peak. This methodology,

* Corresponding author.

0021-9673/96/$15.00
SSDI 0021-9673(95)00437-8

however, is not effective enough to tackle many problems of HPLC optimization, because the optimization based on the precision, $1/s_B$, requires the values of actual error, s_B, for many different integration times, which vary depending on the operating conditions (i.e., peak shape).

Recently, a new theory of uncertainty prediction was advanced [15,16] in which the baseline drift, often formulated as $1/f$ noise (f = frequency), is approximated by the mixture of well known random processes (the white noise and Markov process), permitting the baseline error, s_B, to be calculated based on the probability theory of the time variation in the two random processes. This theory was immediately applied to the following typical problems in analytical chemistry: (1) to determine the optimum time domain for the integration over noisy data in liquid chromatography [17]; (2) to select the horizontal or oblique zero line above which the signal intensities are integrated [17]; and (3) to determine the signal shape at the limit of detection (LOD) for a particular instrument [18].

The above problems are interesting, but not easily solved. At issue is which method of entire area measurement or peak-height measurement provides more precise results in HPLC [4–6,14,19–23]. Although this subject has been disputed over the years, a partial area integration was shown to give better results than either method separately [19,22,23]. The concept of the limit of detection is of fundamental importance in every discipline of analytical chemistry [21,24–36], but over the past 50 years, the academic debate of LOD has been controversial in spectroscopy [24]. The IUPAC recommendations for chromatography [30] cite the minimum detectability that is defined with reference to the signal and noise of the output of the instrument.

The major obstacle to overcome the above problems stems from the actual $1/f$-type fluctuation of the baseline, which differs from the white noise model. That is, the baseline noise displays a strong time dependency. The uncertainty theory, as mentioned above, has been shown to be useful for tackling these problems [15,16]. The aim of this work was to study the applicability and limitations of the theory in practical situations. The error of the prediction itself was also examined. Although the LOD signal and optimum integration were studied separately according to the prediction theory [15,16], the limit of detection for the optimum integration mode is still of interest.

2. Experimental

Naphthalene, acenaphthene, pyrene and perylene were of analytical-reagent grade. A Shimadzu liquid chromatograph was equipped with a photomultiplier tube. The detection wavelength was 254 nm. The sampling intervals of an analogue-to-digital converter were set at 0.2 s and all the HPLC output was stored on the hard disk of a personal computer for batch analysis. The details of the experimental conditions have been described elsewhere [15].

3. Limit of detection and uncertainty prediction theory

The well known definition of LOD is the lowest concentration level or the smallest measurement, x_L, that can be determined to be statistically different from a blank with mean, $\bar{x}_B$, and standard deviation, s_B [24–26]:

$$x_L = \bar{x}_B + \lambda_D s_B \tag{2}$$

where λ_D denotes an arbitrary value which should be chosen in accordance with the confidence level desired. Usually in instrumental analyses, the signal is background subtracted and the mean, $\bar{x}_B$, can be zero:

$$x_L = \lambda_D s_B \tag{3}$$

The variation of the blank measurements is assumed to have a normal distribution. Here, λ_D is fixed at 3. This means that the smallest detectable signal, x_L, is $3s_B$ above the average

baseline ($\bar{x}_B = 0$), and that the probability that a measurement equal to or greater than x_L would be the result of a random fluctuation of the blank signal is 0.13% (the error of the first type, α).

There are many error sources which are reflected in s_B, e.g., sample preparation error, instrumental error and error from calibration lines. Here, we consider the instrumental error only. Situations often arise in which the sample concentration is so low that all the error can be attributed to the baseline noise. If the blank error, s_B, is determined from some appropriate experiments, it is easy to calculate the LOD signal according to Eq. 3. In chromatography, measurements are usually expressed as peak height or area. The constant, λ_D, is dimensionless and the dimension of the error, s_B, should be equal to that of the signal, x_L. This dimensional harmony implies that the blank error should be the S.D. of the "false" peak height or area created by the baseline drift.

The S.D. of the false measurements ($= s_B$) corresponds to the S.D. of the integration results over a time period of the baseline without the analyte signals. We first specify the mode of integration (see Fig. 1). The signal intensities are always gauged from the zero line and are summed over the domain ($k_c + 1$, k_f). The zero line is horizontal (broken line) or oblique (solid line), the statistical superiority of which depends on the stochastic properties of the baseline (see below). The horizontal zero line segment is drawn from the observed intensity at the zero point, k_0. The oblique zero line is drawn between the observed intensities at the edges of the region, k_0 and k_e. The peak-height measurement is an extreme example of the integration with an integration domain of one point.

The baseline statistics can be predicted by the uncertainty theory of chromatography. Fig. 2 illustrates the entire scheme of the theoretical uncertainty prediction. First, the baseline is Fourier transformed into the power spectrum which denotes the power (or squared amplitude) of a wave involved in the baseline as a function of frequency. The power spectrum, $P(k)$, is dissolved into the white noise and Markov process by using the linear least-squares fitting [15]:

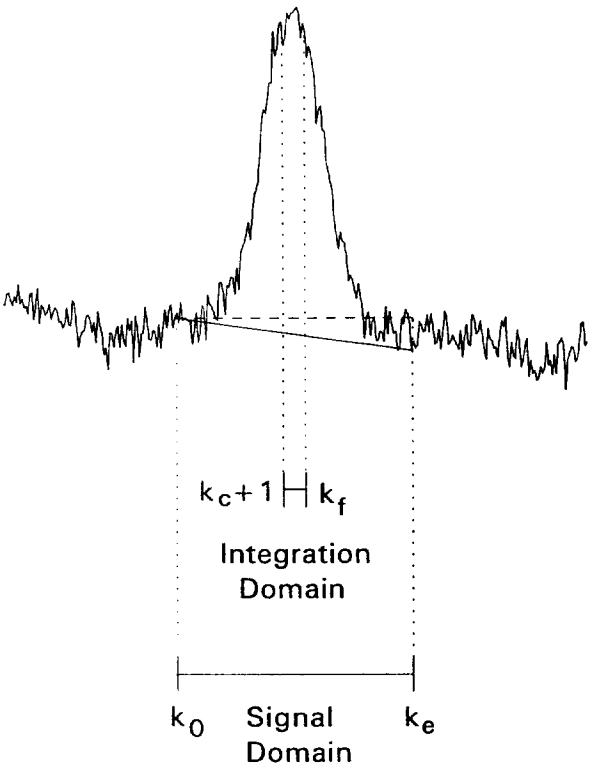

Fig. 1. Example of optimum integration domain. The signal is a Gaussian peak with σ of 15 data points and entire peak area, A_T, of 10 089. The noise is an actual HPLC baseline. k_c denotes cut-off point, k_f filter-off point and the integration domain is $k_c - k_f$. k_0 denotes zero point, the measurement at which is adopted as the zero signal. k_e denotes the end-point. The oblique solid line is drawn from the measured intensity at the zero point to the intensity at the end-point. The noise parameters are $\tilde{w} = 6.11$, $\tilde{m} = 6.63$ and $\rho = 0.977$. In this situation, the optimum integration domain is 11 data points as shown in the figure (R.S.D. = 5.6%).

$$P(k) = \frac{2\tilde{m}^2}{(1+\rho)[(1-\rho)^2 + 4\pi^2(k/N)^2]} + \tilde{w}^2 \quad (4)$$

where k is the number (frequency) used in the Fourier transform. The first term on the right-hand side of Eq. 4 is the theoretical power spectrum of the Markov process and the second term is that of the white noise. In this step, three parameters [S.D. of white noise ($\tilde{w}$), S.D. of Markov process ($\tilde{m}$) and degree of auto-correlation of the Markov process (ρ)] are estimated.

The S.D. of the false area or height created by the white noise and Markov process can be

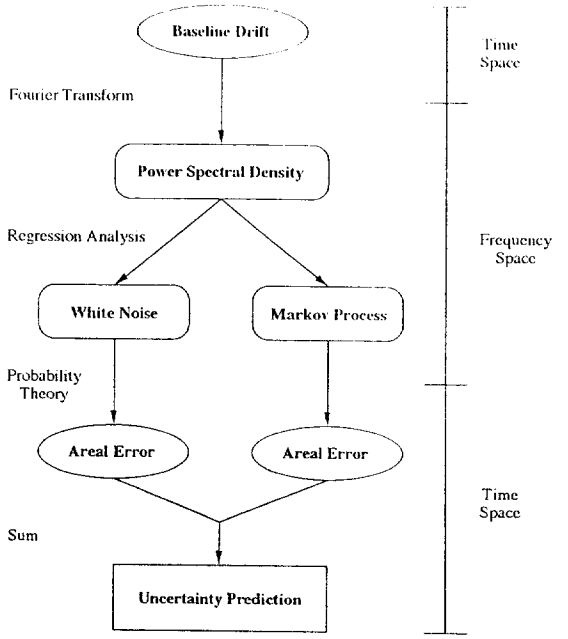

Fig. 2. Procedure for calculating blank S.D.

calculated by the following equation with the noise parameters ($\tilde{w}$, $\tilde{m}$ and ρ) and integration parameters (k_0, k_c, k_f and k_e) [17]:

$$
\begin{aligned}
s_B^2 = {} & (k_f - k_c)\tilde{w}^2 && \text{(first term)} \\
& + \frac{1}{(1-\rho)^2}\left[k_f - k_c - 2\rho \cdot \frac{1-\rho^{k_f-k_c}}{1-\rho}\right. \\
& \left. + \rho^2 \cdot \frac{1-\rho^{2(k_f-k_c)}}{1-\rho^2}\right]\tilde{m}^2 && \text{(second term)} \\
& + \rho^2 \cdot \frac{1-\rho^{2k_c}}{1-\rho^2}\left(\frac{1-\rho^{k_f-k_c}}{1-\rho}\right)^2 \tilde{m}^2 \\
& && \text{(third term)} \\
& + \alpha^2 \tilde{w}^2 && \text{(fourth term)} \\
& + \left\{\alpha^2 \frac{1-\rho^{2k_e}}{1-\rho^2} - 2\alpha\left[\frac{1-\rho^{k_f-k_c}}{1-\rho} \cdot \rho^{k_e+k_c-1}\right.\right. \\
& \cdot \frac{1-\rho^{-2k_c}}{1-\rho^{-2}} + \sum_{i=1}^{k_f-k_c}\left(\frac{1-\rho^{k_f-k_c+1-i}}{1-\rho}\right. \\
& \left.\left.\left. \cdot \rho^{k_e-k_c-i}\right)\right]\right\}\tilde{m}^2 && \text{(fifth term)} \\
& + A^2 I^2 && \text{(sixth term)} \qquad (5)
\end{aligned}
$$

where

$$\alpha = \frac{(k_f - k_c)(k_f + k_c + 1)}{2k_e} \qquad (6)$$

The first term of Eq. 5 denotes the error from the white noise in the integration domain ($k_f - k_c$ data points); the second term, the error from the Markov process in the integration domain ($k_f - k_c$ data points); the third term, the influence of the lag time during k_c data points (if $k_c = 0$, this term is zero); the fourth term, the effect of the white noise in the oblique zero line; the fifth term, the effect of the Markov process in the oblique zero line; and the sixth term, the independent error (mainly originating from the injection error). The fourth and fifth terms should be neglected (= 0) for the horizontal integration.

The auto-correlation coefficient for the white noise and Markov process can be described (for the derivation, see Appendix):

$$\frac{E[r(t)r(t+\tau)]}{\sqrt{E[r(t)^2]E[r(t+\tau)^2]}} = \frac{\rho^\tau\left(\frac{1}{1-\rho^2}\right)\tilde{m}^2 + \delta(\tau)\tilde{w}^2}{\frac{1}{1-\rho^2}\cdot\tilde{m}^2 + \tilde{w}^2} \qquad (7)$$

where τ denotes the lag time and $\delta(\tau)$ the delta function (= 1 if $\tau = 0$ and = 0 if $\tau \neq 0$). This equation can be used for determining the noise parameters, $\tilde{m}$, ρ and $\tilde{w}$, of the baseline instead of Eq. 4. The superiority of the Fourier transform and auto-correlation function is discussed in the parametrization later in this paper.

4. Results

The S.D. of the false measurements of the baseline ($= s_B$) can be obtained experimentally from the real baseline. The random location of the zero point, k_0, and integration domain ($k_c + 1, k_f$) on the sufficiently long baseline leads to the statistic s_B. The zig-zag lines in Fig. 3 show that the baseline S.D. of the false height (A) and area (B) increases with increasing lag time, k_c (where $k_c + 1 = k_f$), and integration period,

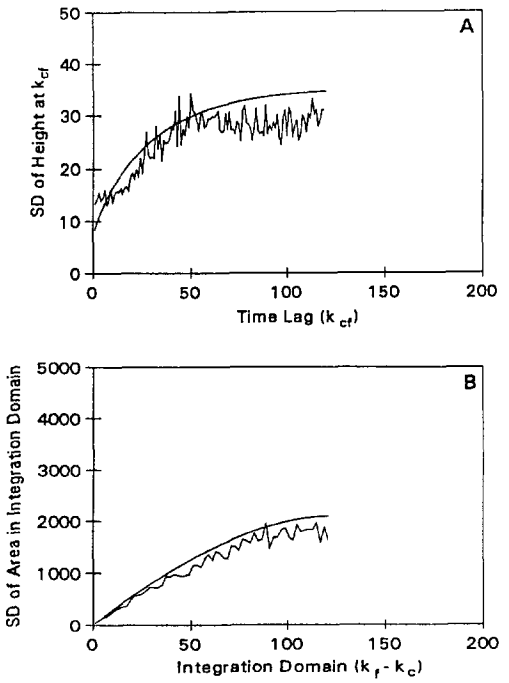

Fig. 3. Statistics of baseline drift with the oblique zero line. (A) S.D. of observed values in the case of peak-height measurement; the abscissa denotes the time to the peak centre, k_{cf}; (B) S.D. of baseline measurements in the case of integration; the abscissa denotes the integration domain ($k_f - k_c$ data points); the time to the peak centre is fixed at 60 data points from the zero point. The periods over which the S.D. is calculated are chosen by the random sampling from the baseline drifts observed (see noise in Fig. 8). The average of 100 S.D. values is plotted.

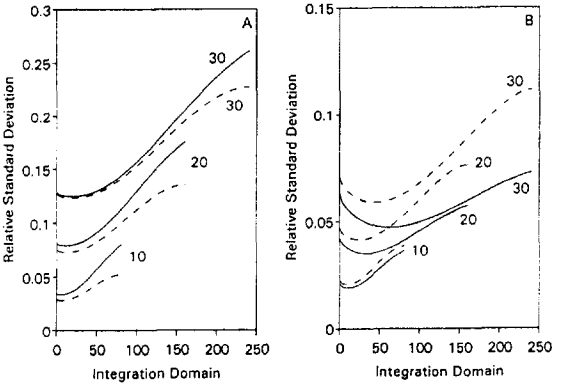

Fig. 4. Dependence of precision on peak width in different baselines ρ = (A) 0.99 and (B) 0.95. — = horizontal zero line; --- = oblique zero line. The figures indicate the peak width, σ (S.D. of a Gaussian peak). $\tilde{w} = 5$; $\tilde{m} = 5$; $k_{cf} = 61$; integration domain = $k_l - k_c$ (symmetrical around the peak centre, k_{cf}); $A_T = 20\,000$. Zero point, k_0 (= 0), and end-point, k_c (=121), are 4σ away from the peak centre.

$(k_c + 1, k_f)$, respectively. It is the smooth lines in Fig. 3 that are theoretically predicted from the power spectral density of the instrumental background as shown in Fig. 2. The injection error, I, is omitted in this calculation, because this error is accompanied by the analyte signal (see Eq. 5). The theoretical prediction of the instrumental uncertainty coincides with the observed uncertainty.

Before applying the theory to actual HPLC analysis, we consider the mathematical properties of the random processes and the dependence of the precision on the integration domain and the peak width, σ, and the degree of auto-correlation, ρ, of the baseline (Fig. 4). The integration with the horizontal zero line (---) and oblique line (—) is also taken into account. The ordinate, R.S.D., means the baseline S.D. divided by the signal area, A [= (s_B^2 of Eq. 5)$^{1/2}$/A; $I = 0$]. Irrespective of the integration modes, peak width and auto-correlation degree, there is an R.S.D. minimum at an integration domain for every line. The optimum time domain which is

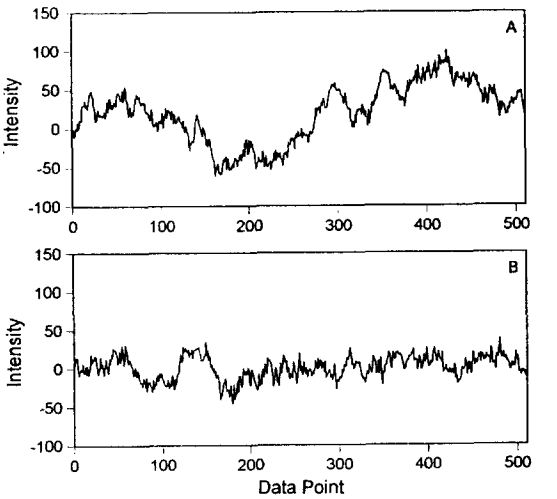

Fig. 5. Baselines with strong auto-correlation (A) ($\rho = 0.99$) and weak auto-correlation (B) ($\rho = 0.95$). $\tilde{w} = 5$; $\tilde{m} = 5$.

characterized by the R.S.D. minimum increases with increasing peak width.

The auto-correlation of the baseline exerts an important influence on the integration precision. The amplitudes of low frequencies in the baseline drift with a high value of ρ (= 0.99 in Fig. 4A) are larger than those with a low value of ρ (= 0.95 in Fig. 4B). Therefore, the time variation of the former baseline appears to be more undulating than the latter baseline. This difference in time space is illustrated in Fig. 5. The low frequencies are known to be harmful for the precise analysis and the R.S.D. lines for $\rho = 0.99$ in Fig. 4 are higher than the corresponding lines for $\rho = 0.95$ (note that the scales of the ordinates are different). The oblique line

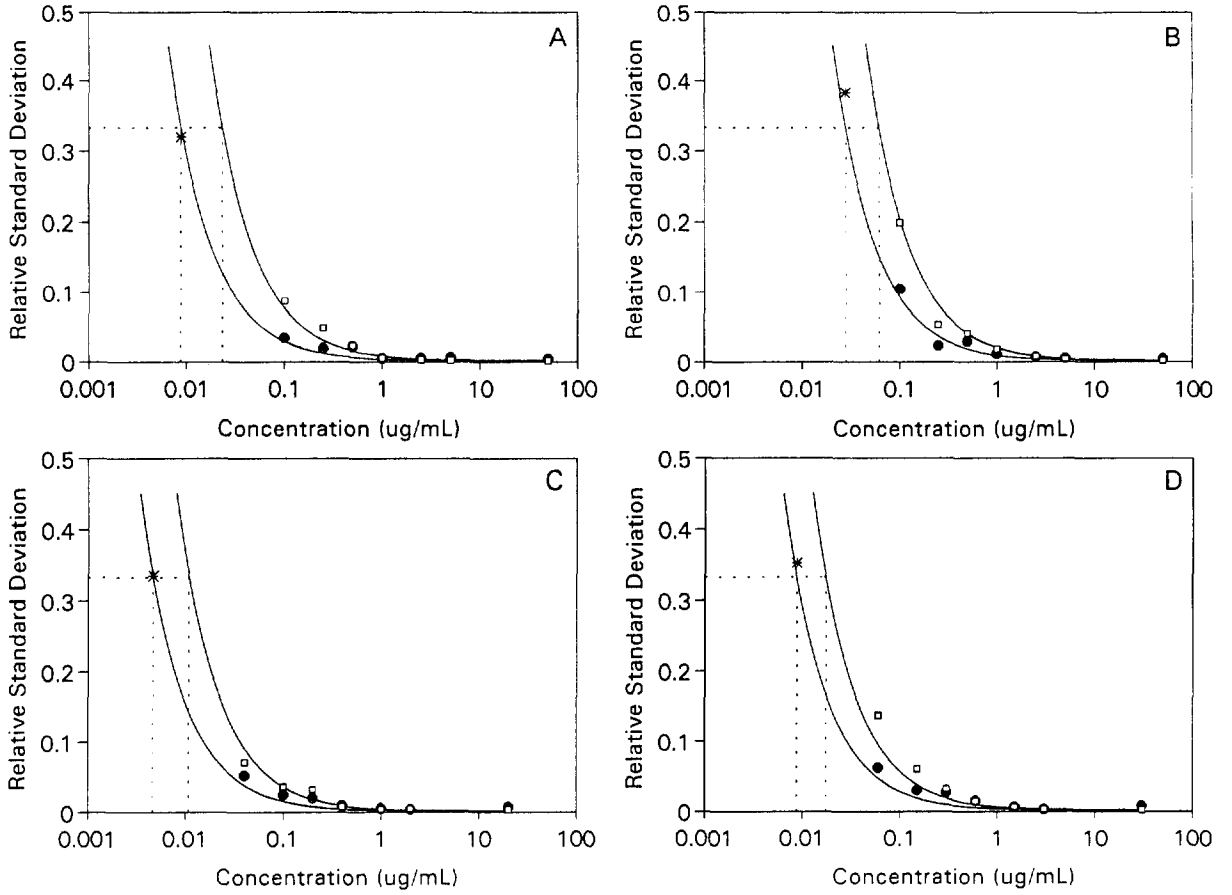

Fig. 6. Dependence of precision on analyte concentration for integration in entire peak region and optimum domain (horizontal zero line). Symbols denote the observed R.S.D.: □ = regular integration; ○ = optimum integration; * = result from the Monte Carlo simulation with the real peak (see Fig. 5 in Ref. [15]) and real baseline shown in Fig. 8. The solid line on the right-side are obtained from the integration over the entire peak region and those in the left-hand side from the optimum integration (Eq. 5). The dotted lines denote LOD. Analyte: (A) for naphthalene (A_T = 14 540 000; σ = 12.3; 50 μm/ml); (B) for acenaphthene (A_T = 5 465 000; σ = 14.4; 50 μm/ml); (C) pyrene (A_T = 15 640 000; σ = 16.6; 20 μm/ml); (D) perylene (A_T = 17 480 000; σ = 22.9; 30 μg/ml). The experimental conditions are described in Ref. [15]. The entire region integration: $k_c = k_0 = 0$; $k_f = k_e$ = (A) 120, (B) 120, (C) 160 or (D) 200. Optimum integration: k_{cf} = (A) 38, (B) 43, (C) 55 or (D) 81; k_c = (A) 120, (B) 120, (C) 140 or (D) 200; $k_f - k_c$ = (A) 9, (B) 11, (C) 15 or (D) 25 (symmetrical around the maximum peak position, k_{cf}). The optimum integration domain is calculated from the assumption of Gaussian peak shape. L.O.D.: A_T = (A) 2575, (B) 3061, (C) 3630 or (D) 5058 (from Eq. 5).

integration (---) is effective when the auto-correlation of the baseline is strong ($\rho = 0.99$), but the horizontal line integration (—) is useful for the baseline with high vibration ($\rho = 0.95$). The R.S.D. for the entire area integration ($\pm 4\sigma$) is almost twice that for the optimum integration for $\rho = 0.99$. The experimental verification for these results has been given elsewhere [18].

We consider the LOD signal for the optimum integration. If the blank S.D. is equal to the S.D. of analyte measurements at a low concentration range [1,2], the background-subtracted signal, x_L, of 33.3% R.S.D. corresponds to the LOD signal ($\lambda_D = 3$):

$$\frac{1}{\lambda_D} = \frac{s_B}{x_L} = \text{R.S.D.}_L \quad (8)$$

Figs. 6 and 7 show the precision–concentration relationship for naphthalene, acenaphthene, pyrene and perylene for the integration with the horizontal line and oblique line, respectively, in HPLC. The dotted lines indicate the LOD signals. The integration results for the optimum domain (○) and entire peak area (□) are also shown in Figs. 6 and 7. The solid lines are drawn according to the uncertainty theory (Eq. 5). Under the HPLC conditions examined, no substantial difference between the integration of the

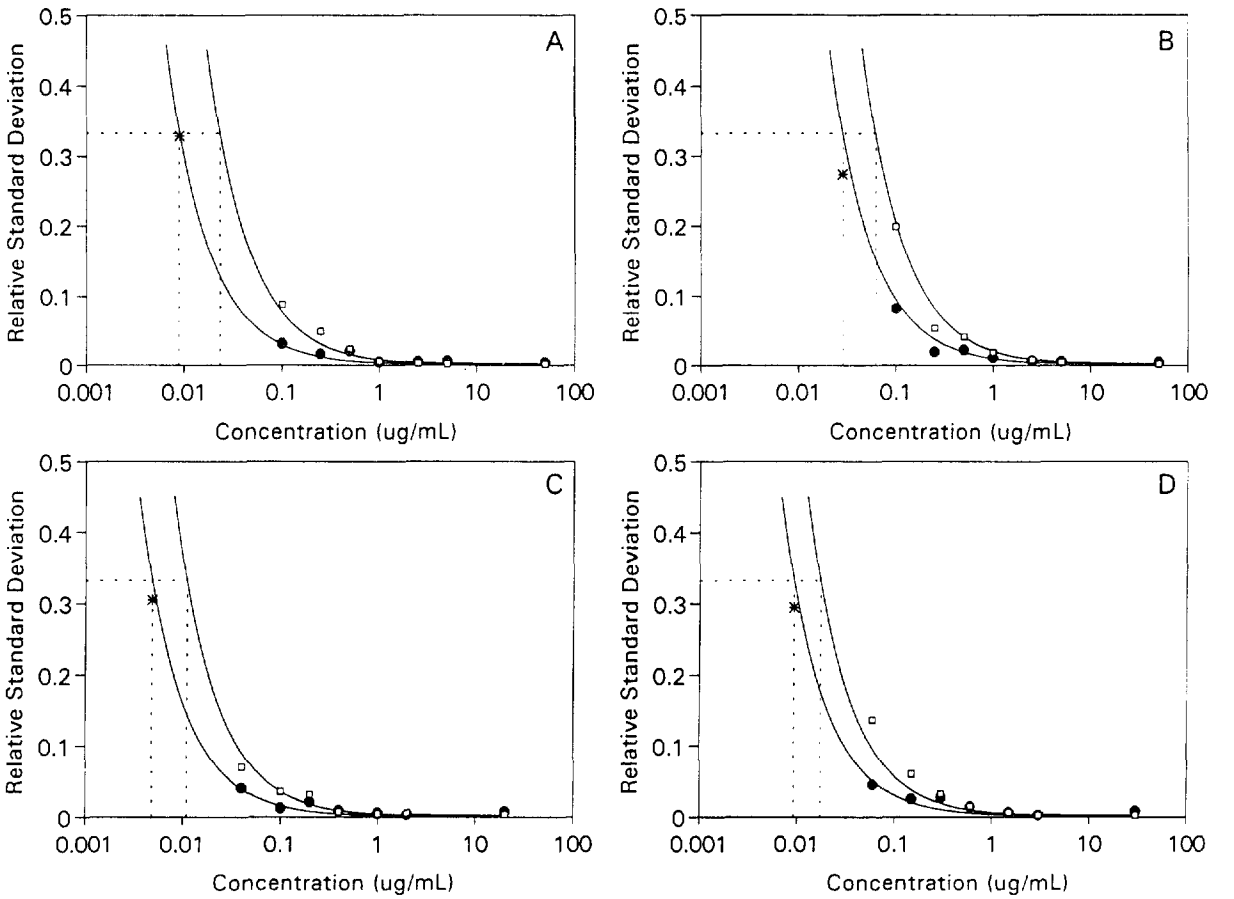

Fig. 7. Dependence of precision on analyte concentration for integration in entire peak region and optimum domain (oblique zero line). Conditions as in Fig. 7 except for the following: optimum integration: $k_f - k_c$ = (A) 9, (B) 11, (C) 13 or (D) 21. LOD: A_T = (A) 2618, (B) 3118, (C) 3759 or (D) 5412.

horizontal and oblique lines can be found. In addition, a capillary electrophoresis apparatus (Photal, Otsuka Electronics) shows the superiority of the horizontal integration because the baseline is dominated by the white noise (not shown).

The experimental results (○ and □) correspond well with the theoretical curves in Figs. 6 and 7. However, the same experimental strategy is not effective for the LOD concentration, which should be characterized by 33% R.S.D. Statistics indicate that a large scattering of the R.S.D. values will be observed (see below). The 95% confidence interval for even 100 replicate experiments is still large around 33% R.S.D. (29.3–38.8). Therefore, Monte Carlo simulation with the real baseline and peak shape was adopted to prove the uncertainty theory. The peak with the amplitude which is predicted to show 33% R.S.D. in theory is randomly placed on the long baseline and the observed R.S.D. is plotted against the theoretical concentration of 33% R.S.D. as shown in Figs. 6 and 7 (*). The computer experiments led to the conclusion that the theoretical prediction of LOD signal is reliable.

As mentioned above, the LOD signal can be calculated directly from Eq. 5. For example, if the zero point is 60 data points away from the peak maximum and if the integration domain covers 40 data points around the peak maximum, the blank S.D., s_B, is ca. 1000 (see the smooth line in Fig. 3B) and then the LOD peak area, x_L, over the integration domain is ca. 3000 ($\lambda_D = 3$; see Eq. 3). Note that the blank S.D. is of areal dimensions in this situation. The LOD signals superimposed over the actual HPLC baseline are illustrated in Fig. 8.

Fig. 9 shows the parametrization error for the baseline drifts and the error of the false area calculated based on these parameters. The noise parameters can be obtained from the power spectrum of the observed baseline as shown in Fig. 2. Of course, some equivocality is accompanied by the parameters. Fig. 9 shows the distributions of the noise parameters (A, $\tilde{m}$; B, ρ; C, $\tilde{w}$; D, s_B) determined from 1000 computer-generated baselines with $\tilde{m} = 5$, $\rho = 0.95$, $\tilde{w} = 10$ and $s_B = 305$. Each baseline is made up of 2048

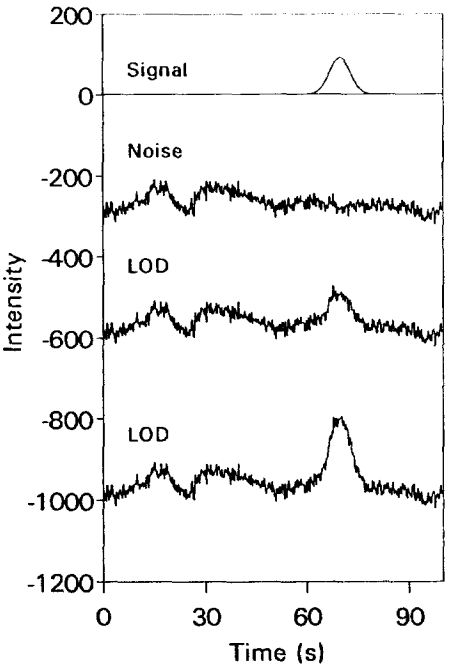

Fig. 8. Noise and signal at the limit of detection. Signal: Gaussian peak with σ of 3 s (15 data points), peak centre of 70 s and peak area of 3363; the zero point and end point are 4σ away from the peak centre. Noise: that observed in an HPLC apparatus. Upper and lower LODs are for optimum integration domain and for the entire area integration, respectively (R.S.D. = 33.3%). Upper LOD: the integration period is $\pm 1/3\sigma$ (11 data points) around the peak centre; the end-point is 121 from the zero point; the signal is the same as the top line. Lower LOD: the integration domain is $\pm 4\sigma$ (121 data points) around the peak centre; peak area = 6823.

data points and 1023 frequencies are evaluated in the power spectrum. The mean and standard deviation of the parameters are listed in Table 1. The relative standard deviations of these parameter distributions are 20% for $\tilde{m}$, 2% for ρ, 13% for $\tilde{w}$ and 10% for s_B. Although the noise parameters vary widely, the scatter of the false area, s_B, is not so large. This is because of the strong correlation of the parameters determined by the simplex least squares of the power spectra (see Table 1).

Let us consider the experimental determination of the LOD signal. The concentration which would provide 33% R.S.D. of measurements should be searched for. Statistics clearly illustrates this difficulty. If the mean of 100 and S.D.

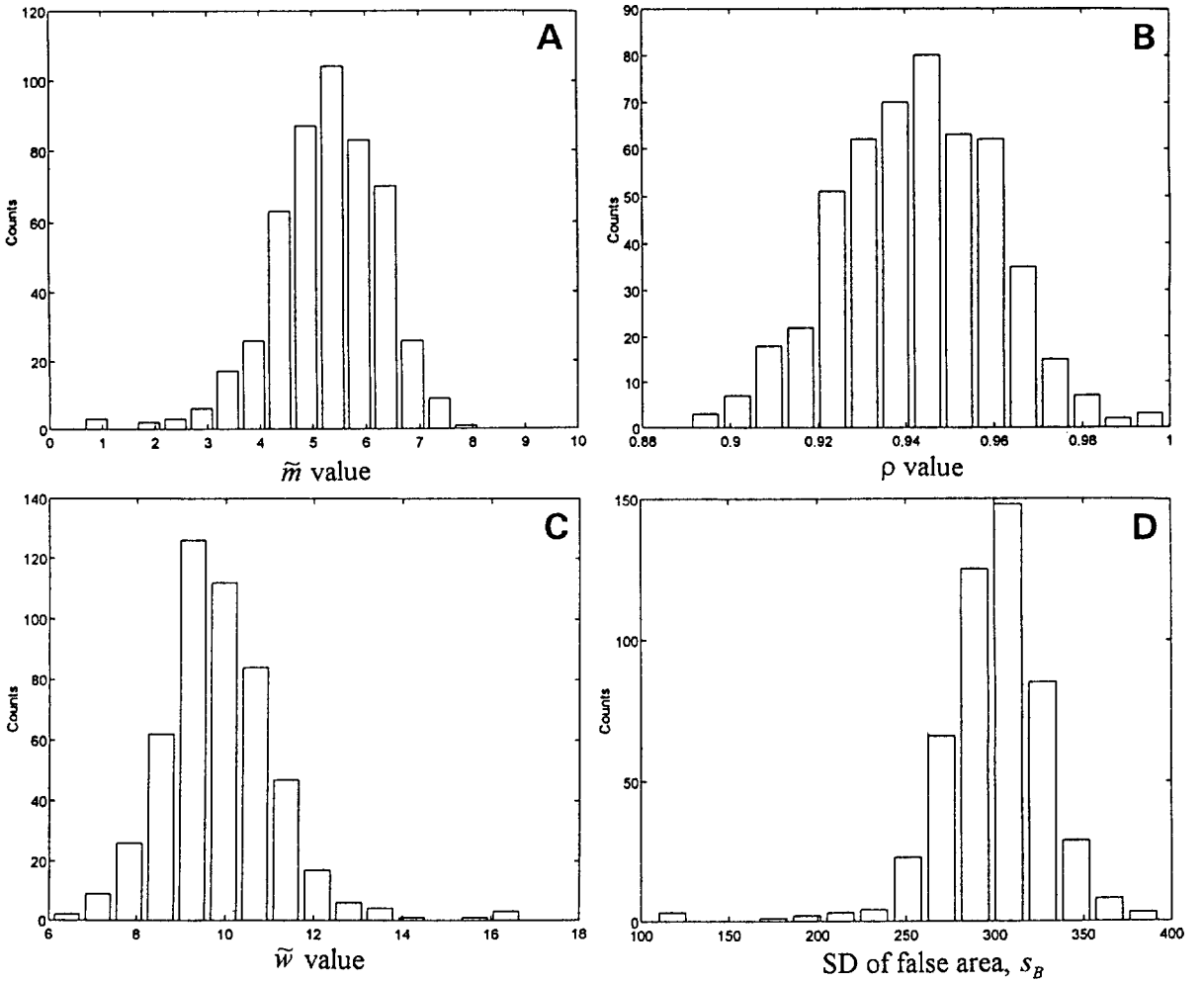

Fig. 9. Distributions of (A–C) parametrization and (D) S.D. of false area. 1000 replicate baselines are used for the parametrization statistics. 1000 sets of parameters ($\tilde{w}$, $\tilde{m}$ and ρ) are obtained from each baseline generated by the computer and the S.D. of the false area is obtained from each set of the parameters. $k_c = 1$; $k_f = 30$. The horizontal zero line is used for the integration.

of 33.3 are obtained from 10 replicate experiments ($n = 10$), the 95% confidence interval of the population S.D. ranges widely from 22.9 to 69.1. The 95% confidence interval for 100 replicate experiments is still large (29.3–38.8). In the uncertainty theory of this paper, ten replicates of the baselines give the 95% confidence interval ranging from 31 to 35 on the same scale. The 95% confidence interval for ten replicates is calculated as $0.333 \pm 1.96 \times 0.333 \times 0.10/\sqrt{10}$. This result clearly demonstrates that the uncertainty theory can estimate the LOD signal more reliably.

The auto-correlation of the baseline can also be used for the parameterization of the baselines. The auto-correlation for the mixed process of the white noise and Markov process is given in Eq. 7. Table 1 also includes the results of the parametrization using the auto-correlation. The Monte Carlo simulation is carried out in the same way as that for the power spectrum (2048 data points of each baseline, but the lag

Table 1
Parametrization by power spectrum and auto-correlation

Correlation coefficient of power spectrum				Parameter	Power spectrum	Auto-correlation
m	1			Mean m	5.2724	5.546
ρ	−0.88	1		S.D. m	1.0304	1.2767
w	−0.94	0.78	1			
	m	ρ	w	Mean ρ	0.9424	0.9406
				S.D. ρ	0.0182	0.0165
Correlation coefficient of auto-correlation				Mean w	9.8699	9.8571
				S.D. w	1.3157	2.9312
m	1					
ρ	−0.45	1		Mean false area	299.4225	312.6429
w	0.2	0.51	1	S.D. false area	31.158	66.0217
	m	ρ	w			

2048 points of time variation data are used for this simulation. The long, gentle slope of the mixed random process is removed by the linear least squares for each set of 2048 data points. For the parametrization, 1024 points are available for the power spectrum and the lag time of the auto-correlation ranges from zero to 203.

time ranges from 0 to 203). Unfortunately, the parametrization by the auto-correlation displays more error. The reason may be the weak correlation between the noise parameters in the parameterization (see Table 1).

5. Discussion

This paper has demonstrated how to calculate the S.D. of false area (or height) created by the baseline which depends on the peak width (or the integration domain). Eq. 5 includes all the fundamental concepts of this uncertainty prediction. All the requirements for the prediction are the actual baseline, smooth peak shape and injection error in HPLC. However, some significant problems should be solved before the uncertainty theory is applied to HPLC optimization.

First, the quantitative relationship between the precision and peak separation should be elucidated. Peak separation is of vital importance in separation science and the precision has universal importance in every discipline of analytical chemistry. The optimization should be performed with close reference to the above relationship. An information–theoretical approach to optimiation will be useful for this purpose. Further, the errors originating from the other steps in an entire chemical analysis such as sample preparation and calibration graph should also be taken into account. Coupled with the quantitative structure–retention relationship, the uncertainty prediction would cover the entire analysis from molecular structure to precision.

Appendix

If the same symbols are used in Ref. [15], the variation at time t and $t+\tau$ can be given as

$$r(t) = \rho^{t-1}m(1) + \rho^{t-2}m(2) + \cdots + \rho m(t-1) + m(t) + w(t) \quad \text{(A1)}$$

$$r(t+\tau) = \rho^{t+\tau-1}m(1) + \rho^{t+\tau-2}m(2) + \cdots + \rho^{\tau+1}m(t-1) + \cdots + \rho m(t+\tau-1) + m(t+\tau) + w(t+\tau) \quad \text{(A2)}$$

The variances of these variations are described as

$$E[r(t)^2] = \frac{1-\rho^{2t}}{1-\rho^2}\cdot\tilde{m}^2 + \tilde{w}^2 \quad \text{(A3)}$$

$$E[r(t+\tau)^2] = \frac{1-\rho^{2(t+\tau)}}{1-\rho^2} \cdot \tilde{m}^2 + \tilde{w}^2 \quad \text{(A4)}$$

The covariance of $r(t)$ and $r(t+\tau)$ takes the form

$$E[r(t)r(t+\tau)] = \rho^{\tau}(\rho^{2t-2} + \rho^{2t-4} + \cdots + \rho^2 + 1)\tilde{m}$$

$$= \rho^{\tau} \cdot \frac{1-\rho^{2t}}{1-\rho^2} \cdot \tilde{m} + \delta(\tau)\tilde{w}^2 \quad \text{(A5)}$$

If t is large (i.e., the stationary phase), the variances and covariance of the random variables at time t and $t+\tau$ are reduced to the simple forms

$$E[r(t)^2] = E[r(t+\tau)^2] = \frac{1}{1-\rho^2} \cdot \tilde{m}^2 + \tilde{w}^2 \quad \text{(A6)}$$

$$E[r(t)r(t+\tau)] = \rho^{\tau} \cdot \frac{1}{1-\rho^2} \cdot \tilde{m} + \delta(\tau)\tilde{w}^2 \quad \text{(A7)}$$

Note that $\rho < 1$. From Eqs. A6 and A7, Eq. 7 can be derived.

References

[1] A.W. Westerberg, Anal. Chem., 41 (1969) 1770.
[2] J.F.K. Huber, J.A.R.J. Hulsman and C.A.M. Meijers, J. Chromatogr., 62 (1971) 79.
[3] L.R. Snyder, J. Chromatogr. Sci., 10 (1972) 200.
[4] H. Barth, E. Dallmeier, G. Courtois, H.E. Keller and B.L. Karger, J. Chromatogr., 83 (1973) 289.
[5] S.R. Bakalyar and R.A. Henry, J. Chromatogr., 126 (1976) 327.
[6] R.P.W. Scott and C.E. Reese, J. Chromatogr., 138 (1977) 283.
[7] I. Halász and P. Vogtel, J. Chromatogr., 142 (1977) 241.
[8] L.R. Snyder and S. van der Wal, Anal. Chem., 53 (1981) 877.
[9] J.P. Foley, J. Chromatogr., 384 (1987) 301.
[10] A.N. Papas and M.F. Delaney, Anal. Chem., 59 (1987) 54A.
[11] E. Grushka and I. Zamir, Chemical Analysis, 1989, Ch. 13.
[12] N. Dyson, Chromatographic Integration Methods, Royal Society of Chemistry, Cambridge, 1990.
[13] Y. Hayashi and R. Matsuda, Chemometr. Intell. Lab. Syst., 18 (1993) 1.
[14] Y. Hayashi and R. Matsuda, Advances in Chromatography, 1994, Ch. 7.
[15] Y. Hayashi and R. Matsuda, Anal. Chem., 66 (1994) 2874.
[16] Y. Hayashi and R. Matsuda, Anal. Sci., 10 (1994) 725.
[17] Y. Hayashi and R. Matsuda, Chromatographia, in press.
[18] Y. Hayashi, R. Matsuda and R.B. Poe, Chromatographia, in press.
[19] Y. Hayashi and R. Matsuda, Anal. Sci., 10 (1994) 553.
[20] R.B. Poe and S.C. Rutan, Anal. Chim. Acta, 283 (1993) 845.
[21] R.E. Synovec and E.S. Yeung, Anal. Chem., 57 (1985) 2162.
[22] T. Hirschfeld, Appl. Spectrosc., 30 (1976) 67.
[23] E.H. Piepmeier, Anal. Chem., 48 (1976) 1296.
[24] P.W.J.M. Boumans, Anal. Chem., 66 (1994) 459A.
[25] G.L. Long and J.D. Winefordner, Anal. Chem., 55 (1983) 712A.
[26] L.H. Keith, W. Crummett, J. Deegan, Jr., R.A. Libby, J.K. Taylor and G. Wentler, Anal. Chem., 55 (1983) 2210.
[27] D. Lambert, B. Peterson and I. Terpenning, J. Am. Stat. Assoc., 86 (1991) 266.
[28] Office of Health Studies. Chemicals in the Environment, 1993.
[29] L.A. Currie, Pure Appl. Chem., 64 (1992) 455.
[30] L.S. Ettre, Pure Appl. Chem., 65 (1993) 819.
[31] L.A. Currie and G. Svehla, Pure Appl. Chem., 66 (1994) 595.
[32] R. Ferrús and M.R. Egea, Anal. Chim. Acta, 287 (1994) 119.
[33] W.J. Taraszewski, D.T. Haworth and B.D. Pollard, Anal. Chim. Acta, 157 (1984) 73.
[34] J.P. Foley and J.G. Dorsey, Chromatographia, 18 (1984) 503.
[35] P. Kaiser, Chromatographia, 4 (1971) 123.
[36] R. Kaiser, Chromatographia, 4 (1971) 215.